Intrinsic and extrinsic corrugation of monolayer graphene deposited on SiO_2

V. Geringer,[1,3] M. Liebmann,[1,3] T. Echtermeyer,[2] S. Runte,[1,3] M. Schmidt,[1,3] R. Rückamp,[1,3] M. C. Lemme,[2] and M. Morgenstern[1,3]

[1]*II. Institute of Physics, RWTH Aachen University, Otto-Blumenthal-Straße, 52074 Aachen, Germany*
[2]*Advanced Microelectronic Center Aachen (AMICA), AMO GmbH, Otto-Blumenthal-Straße 25, 52074 Aachen, Germany*
[3]*JARA: Fundamentals of Future Information Technology, Otto-Blumenthal-Straße, 52074 Aachen, Germany*

(Received 5 June 2008; published 17 February 2009)

Using scanning tunneling microscopy in an ultrahigh vacuum and atomic force microscopy, we investigate the corrugation of graphene flakes deposited by exfoliation on a Si/SiO_2 (300 nm) surface. While the corrugation on SiO_2 is long range with a correlation length of about 25 nm, some of the graphene monolayers exhibit an additional corrugation with a preferential wavelength of about 15 nm. A detailed analysis shows that the long-range corrugation of the substrate is also visible on graphene, but with a reduced amplitude, leading to the conclusion that the graphene is partly freely suspended between hills of the substrate. Thus, the intrinsic rippling observed previously on artificially suspended graphene can exist as well, if graphene is deposited on SiO_2.

DOI: 10.1103/PhysRevLett.102.076102 PACS numbers: 68.55.J−, 68.37.Ef, 68.37.Ps, 68.65.−k

Since it was believed, based on the Mermin-Wagner theorem, that two-dimensional (2D) crystals are not stable at finite temperature [1], it came as a surprise that monolayer graphene could be stabilized on a Si/SiO_2 substrate [2–4]. Because of its peculiar properties such as a linear dispersion leading to Klein tunneling [5], high room-temperature mobility allowing quantum Hall steps at 300 K [6], a low spin-orbit interaction beneficial for spintronic devices [7], or tunable spin-polarized edge states [8], graphene studies have become a major issue in solid-state physics. Already, the first transport results not exhibiting weak localization lead to the speculation of a curved surface [9] acting as a phase-breaking field [10]. Such a curvature was indeed observed by microscopic electron diffraction of suspended monolayer graphene sheets [11]. The lateral wavelength of the isotropic curvature is estimated to be $\lambda = 10$–25 nm with an amplitude of $A \simeq 1$ nm. The rippling has been reproduced theoretically by Monte Carlo simulations with a preferential wavelength of 8 nm, barely depending on temperature [12]. It is argued that the anharmonic coupling between bending and stretching modes in graphene causes the rippling and is responsible for the stability of the 2D crystal. Moreover, it has been shown experimentally that rippling can ultimately limit the mobility of graphene at 300 K, if defects are avoided [13]

However, the corrugation properties of graphene deposited on a substrate as typically used in transport experiments are not clarified. In particular, previous scanning probe studies [14–17] revealed only corrugations, which are attributed to the roughness of the underlying substrate, except for a torn flake manipulated by atomic force microscopy (AFM) [16]. Thus, it is unclear if the intrinsic tendency for rippling persists on the substrate, thereby ultimately limiting mobility and influencing weak localization which has meanwhile been found, at least, for some samples [16]. Here, we demonstrate that a regular short wavelength corrugation with $\lambda \simeq 15$ nm and $A \simeq 1$ nm, which is not induced by the substrate, can even prevail the substrate corrugation. Since λ and A are close to the values found on suspended graphene [11], we attribute this additional corrugation to the intrinsic rippling of graphene [12]. Moreover, we find that the long-range corrugation implied by the substrate has lower amplitude on graphene than on SiO_2, suggesting that our high-mobility graphene is partly suspended between hills of the substrate, which might favor the development of the intrinsic short-scale rippling.

The graphene sample is fabricated by the mechanical exfoliation technique as described in [2,18]. Using an optical microscope, a graphene flake containing a monolayer region is identified. Raman spectroscopy is used to confirm the number of layers with the help of the 2D line [19]. Figure 1(a) shows three spectra measured in different areas of the flake visible in Fig. 1(b). In addition to a large monolayer area, we find smaller bi- and multilayer areas as marked by 1L, 2L, and MuL, respectively. Next, gold contacts with a 10 nm Cr seed layer were deposited and structured with a lift-off process. Except for one side, the graphene sample is completely surrounded by the gold electrode as shown in Fig. 1(b). The mobility of graphene samples prepared identically but with several contacts is $\mu = 1 - 1.5\ m^2/(V\,s)$ at 300 K [20], i.e., comparable with high-mobility values obtained by other groups [13,21]. In order to remove residual resist and adsorbates, the sample was rinsed in isopropanol and acetone, baked out to 150 °C in air for four hours and, additionally, baked out to the same temperature in ultrahigh vacuum (UHV) for three

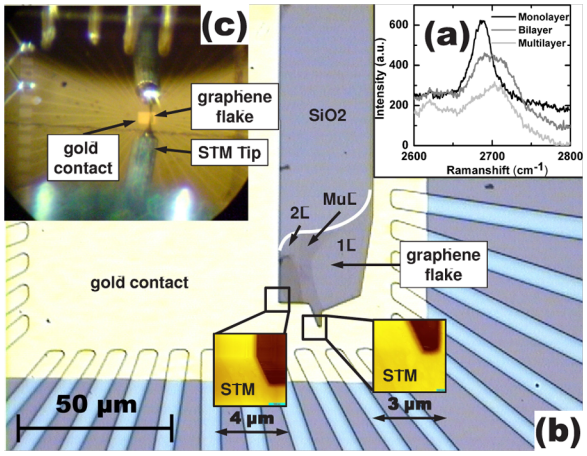

FIG. 1 (color online). (a) Raman spectra using laser light of wavelength 532.1 nm. The spectra are recorded on different areas of the graphene flake and the attribution to monolayer, bilayer, and multilayer is marked. (b) Optical image of the graphene sample with gold contacts. The different areas of monolayer (1L), bilayer (2L), and multilayer (MuL) as identified by Raman spectroscopy are indicated. Insets show two STM images acquired at the edge of the gold contact, which are used for orientation. (c) Microscopic image of the STM tip in tunneling contact with the graphene in UHV recorded with a long-range optical microscope.

hours. The gold film served as the electrical contact for scanning tunneling microscopy (STM) and was used to prepare the STM tip (etched W) by voltage pulses. In order to find the graphene within the UHV-STM, we used an optical microscope with a focal length of 30 cm and 5 μm lateral resolution. Figure 1(c) shows a microscopic image of the tip approaching the graphene flake. The home-built STM features an xy stage for lateral positioning and operates in UHV (2×10^{-7} Pa) as described elsewhere [22,23]. The xy stage has been checked to move accurately within 10%. Topographic images are recorded applying a bias V to the tip. Spectroscopic dI/dV curves are measured by a lock-in technique using a modulation voltage V_{mod} after stabilizing the tip at voltage V_{stab} and current I_{stab}. STM images obtained at the intentionally irregular edge of the gold contact are displayed in the insets of Fig. 1(b). They are used for orientation by STM and aid in finding monolayer, bilayer, and multilayer areas on the flake.

Atomic force microscopy images are taken under ambient conditions in the tapping mode using either a commercial cantilever with a silicon tip or an ultrasharp tungsten tip with a tip radius of 1 nm, which is attached at the bottom of a Si cantilever [24]. Imaging has been carried out in the attractive regime [25] with an oscillation frequency slightly above resonance.

Figures 2(b) and 2(c) show two atomically resolved STM images recorded on the monolayer (1L) and the multilayer (MuL) of graphene, respectively. One observes a hexagonal pattern on the monolayer and a triangular pattern on the multilayer in accordance with previous results [14,17]. The atomic resolution is still perceptible at lower resolution in Figs. 2(a) and 2(d), but an additional irregular corrugation appears. Line sections shown in Fig. 2(e) reveal that the corrugation height on this monolayer region is about 0.6 nm, a factor of 3 larger than on the multilayer region. Notice that corrugation heights pretended by charged defects are typically smaller by more than an order of magnitude [26]. A representative $dI/dV/(I/V)$ curve of the monolayer, which is known to represent the local density of states [27], is shown in Fig. 2(f). As expected for graphene, it shows a V-like shape with the Dirac point at about $V = -20$ mV. It does not change significantly across the area depicted in Fig. 2(d). Note that graphene on SiC(0001) exhibits a more complicated dI/dV spectrum [28–30]. Note also, that we did not observe the phonon gap found at 4 K recently [17], although we used several different micro- and macrotips. This is tentatively attributed to the different temperature of the two experiments. The good representation of the graphene local density of states by $dI/dV/(I/V)$ and the continuous atomic resolution across Fig. 2(d) demonstrates the absence of resist on this part of the surface. Indeed, we found several large areas without resist, but still also areas

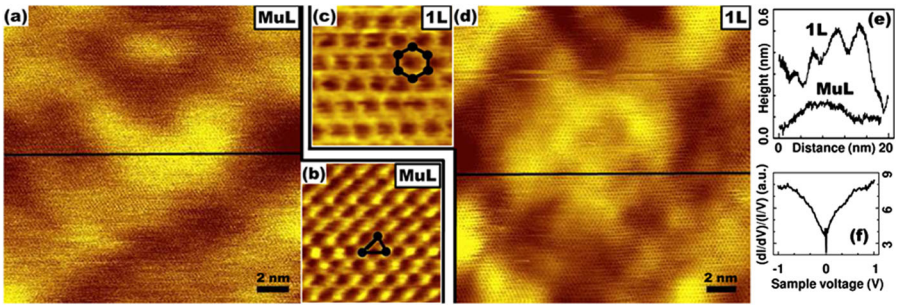

FIG. 2 (color online). (a) Constant current STM image of multilayer graphene (0.4 V, 258 pA) (raw data). (b) Higher resolution STM image of the same area as in (a) with triangular atomic structure indicated (0.4 V, 198 pA). (c) High resolution STM image of graphene monolayer area with hexagonal atomic structure indicated (1 V, 394 pA). (d) Lower resolution STM image of monolayer graphene (0.5 V, 292 pA) (raw data). (e) Line section along the lines depicted in (a)(MuL) and (d)(1L). (f) Normalized dI/dV spectrum of monolayer graphene: $V_{\mathrm{stab}} = 0.7$ V, $I_{\mathrm{stab}} = 300$ pA, $V_{\mathrm{mod}} = 20$ mV.

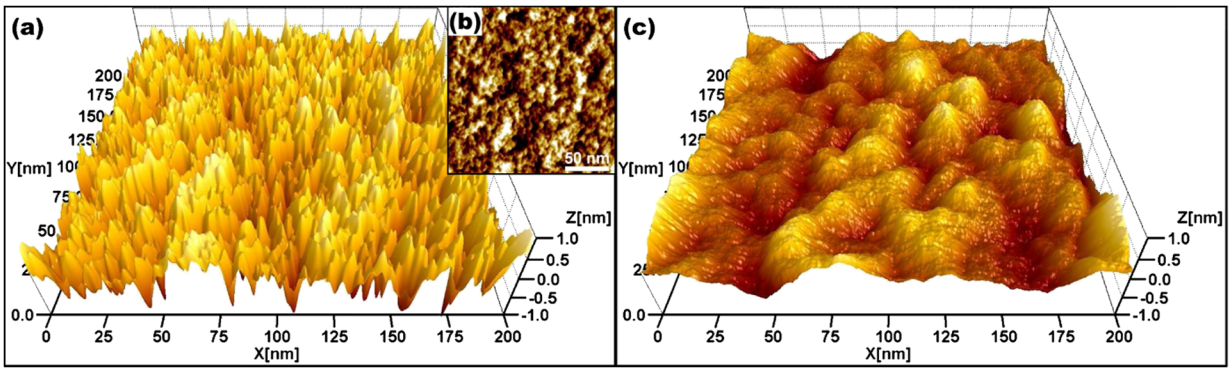

FIG. 3 (color online). (a), (b) 3D and 2D constant current STM image of monolayer graphene (1 V, 207 pA). (c) 3D tapping mode AFM image of the SiO_2 substrate (resonance frequency 326.4 kHz, force constant 47 N/m, excitation frequency 326.5 kHz, oscillation amplitude 18 nm, constant amplitude feedback, set point 90%). Note the identical scale of both images.

where a remaining resist is apparent within the STM images. The fact that the Dirac point is observed close to 0 V shows a negligible influence of charging adsorbates, which are probably removed in UHV.

Figure 3(a) shows a large area STM image of the graphene monolayer. One observes a rather regular corrugation with amplitudes of more than 1 nm and a preferential distance between hills of about 15 nm. The histogram [31] is Gaussian with a full width at half maximum (FWHM) of 0.78 nm. The rms roughness is 0.36 nm. The latter two values fluctuate across the monolayer area by about 25% (average rms roughness 0.32 nm), but the corrugation length scale remains constant. For comparison, Fig. 3(c) shows an AFM image of the bare SiO_2 surface recorded in tapping mode. It is obvious that the corrugation on the substrate is lower in height and exhibits a larger length scale than the corrugation on graphene. The FWHM of the histogram of Fig. 3(c) is 0.48 nm and the rms roughness is 0.22 nm [average (0.25 ± 0.05) nm]. We used four different tips, including two ultrasharp tips with a tip radius of 1 nm [24], but always observed the same corrugation height and length scale, which, in addition, is in good agreement with previous results [15].

Careful inspection of the graphene monolayer in Figs. 3(a) and 3(b) shows a modulation on top of the short-range corrugation exhibiting a similar length scale as the corrugation on the SiO_2 substrate. In order to disentangle the two contributions, we used two-dimensional autocorrelation functions of the images (a) and (c) [32], which are shown in Figs. 4(a) and 4(b). Note that both figures use the same color scale; i.e., the intensities are directly comparable. A long-range structure represented by a central spot surrounded by four bright areas is visible in both images, although with weaker intensity for graphene (a). Figure 4(c) shows the autocorrelation function of the graphene after removing the long-range part by high-pass filtering using a smooth (first order Butterworth) cutoff at wavelength $\lambda = 20$ nm. A preferential short-range distance is clearly visible by the strong spots around the center, but there is additional multiple correlation, albeit not with high symmetry. Notice that creep and drift effects are carefully removed from the STM image using the atomic resolution. We checked the preferential directions visible in both correlation patterns. They are rotating arbitrarily across the SiO_2, but we find indication for a preferential orientation on graphene [31]. Figure 4(d) shows radial line sections averaged over all angles of the correlation functions. The SiO_2 (black curve) exhibits a correlation length of about 25 nm comparable to [15] and, in addition, a very weak maximum at about 50 nm indicating a slight preferential distance between hills. The gray curve shows the radial line section of the high-pass filtered image of graphene visible in Fig. 4(c). It exhibits a damped oscillation with a wavelength of about 14 nm looking very similar to correlation functions of liquids. For com-

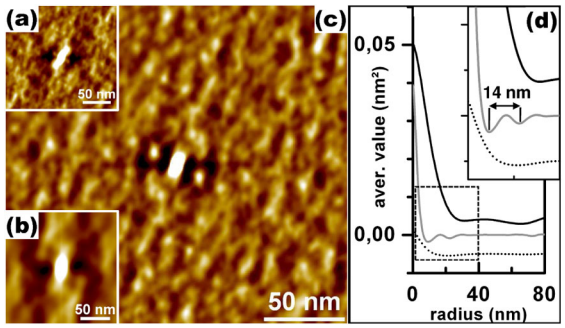

FIG. 4 (color online). (a) 2D autocorrelation function of the drift corrected STM image of monolayer graphene as shown in Fig. 3(a). (b) 2D autocorrelation function of the AFM image of the SiO_2 surface as shown in Fig. 3(c), same color scale as in (a). (c) Fast Fourier transform high pass filtered image (1 order Butterworth, 20 nm) of the 2D autocorrelation function shown in (a). (d) Radial line sections of the unfiltered autocorrelation image (b) (black line), of the high pass filtered autocorrelation image (c) (gray line), and of the high pass filtered autocorrelation image to Fig. 3(c), which is not shown (dotted line). The inset shows a larger view of the area marked by the dashed line. The black and gray graphs are offset vertically for clarity.

parison, the radial line section of the autocorrelation function of the SiO_2 image after applying the same high-pass filter is shown as a dotted line and does not exhibit any structure. We observe the damped oscillation also after high-pass filtering the original STM image of graphene in Fig. 3(a) and determining the autocorrelation function afterwards. In addition, we checked that the obtained wavelength is quite robust with respect to slight parameter changes of the filtering process. Depending on the filtering procedure and the selection of the minima or maxima used for determining the wavelength, λ is varying by at maximum ± 2 nm with a mean value of $\lambda = 15$ nm.

From these results, we conclude that monolayer graphene can exhibit a rather regular, liquidlike short-scale corrugation not induced by the substrate. It is similar in height and wavelength to the one observed on suspended graphene [11] and calculated for freely suspended graphene by atomic Monte Carlo methods [12]. This observation suggests that the graphene might be partly suspended even on the SiO_2. In order to verify this, we compared the Fourier components of the images of graphene and SiO_2 within the large wavelength's region $\lambda =$ 40–60 nm [31]. We indeed find that graphene exhibits an up to 40% lower amplitude at all wavelengths within this wavelength range. This implies that the graphene does not follow the substrate corrugations exactly, but instead includes areas not in contact with the substrate. We believe that this partly free-standing configuration is the prerequisite for the intrinsic rippling of graphene. Indeed, we have also found other graphene flakes prepared nominally identically by the same person, which did not show the intrinsic rippling. This highlights that tiny details of the preparation process can have large impacts on the physical properties, maybe explaining the contradicting weak localization properties in different studies [9,16]. A comparison of Raman data of several samples indicates that samples with intrinsic rippling are more frequent than samples without [31].

In summary, we have investigated high-mobility graphene flakes on SiO_2 by UHV-STM and scanning tunneling spectroscopy. A mesoscopic corrugation not induced by the substrate is identified. It is rather regular exhibiting liquidlike correlation properties with a preferential wavelength of about 15 nm and a rms roughness of 0.32 nm. Since the long-range corrugation of the substrate is additionally visible on graphene, but with smaller amplitude than on the substrate, we conclude that the rippled graphene is partly freely suspended.

We gratefully acknowledge useful discussions with G. Güntherodt, U. D. Schwarz, and H. Kurz and financial support by FOR 912, project TP 6 of the Deutsche Forschungsgemeinschaft and by the German Federal Ministry of Education and Research (BMBF) under Contract No. NKNF 03X5508 (“ALEGRA”).

[1] N. D. Mermin, Phys. Rev. **176**, 250 (1968).
[2] K. S. Novoselov *et al.*, Science **306**, 666 (2004).
[3] Y. Zhang, J. W. Tan, H. L. Stormer, and P. Kim, Nature (London) **438**, 201 (2005).
[4] A. K. Geim and K. S. Novoselov, Nature Mater. **6**, 183 (2007).
[5] M. I. Katsnelson, K. S. Novoselov, and A. K. Geim, Nature Phys. **2**, 620 (2006).
[6] K. S. Novoselov *et al.*, Science **315**, 1379 (2007).
[7] N. Tombros, C. Jozsa, M. Popinciuc, H. T. Jonkman, and B. J. van Wees, Nature (London) **448**, 571 (2007).
[8] Y. W. Son, M. L. Cohen, and S. G. Louie, Nature (London) **444**, 347 (2006).
[9] S. V. Morozov *et al.*, Phys. Rev. Lett. **97**, 016801 (2006).
[10] E. McCann *et al.*, Phys. Rev. Lett. **97**, 146805 (2006).
[11] J. C. Meyer *et al.*, Nature (London) **446**, 60 (2007).
[12] A. Fasolino, J. H. Los, and M. I. Katsnelson, Nature Mater. **6**, 858 (2007).
[13] S. V. Morozov *et al.*, Phys. Rev. Lett. **100**, 016602 (2008).
[14] E. Stolyarova *et al.*, Proc. Natl. Acad. Sci. U.S.A. **104**, 9209 (2007).
[15] M. Ishigami, J. H. Chen, W. G. Cullen, M. S. Fuhrer, and E. D. Williams, Nano Lett. **7**, 1643 (2007).
[16] F. V. Tikhonenko, D. W. Horsell, R. V. Gorbachev, and A. K. Savchenko, Phys. Rev. Lett. **100**, 056802 (2008).
[17] Y. Zhang *et al.*, Nature Phys. **4**, 627 (2008).
[18] M. C. Lemme, T. J. Echtermeyer, M. Baus, and H. Kurz, IEEE Electron Device Lett. **28**, 282 (2007).
[19] A. C. Ferrari *et al.*, Phys. Rev. Lett. **97**, 187401 (2006).
[20] M. Lemme *et al.*, Solid-State Electron. **52**, 514 (2008).
[21] Y. W. Tan *et al.*, Phys. Rev. Lett. **99**, 246803 (2007).
[22] J. Wiebe *et al.*, Rev. Sci. Instrum. **75**, 4871 (2004).
[23] T. Mashoff, M. Pratzer, and M. Morgenstern(to be published).
[24] MikroMasch (www.spmtips.com), NSC15 (Si) and DP15/HiRes-W/AlBS (Si cantilever with W tip apex).
[25] H. Hölscher and U. D. Schwarz, Int. J. Non-Linear Mech. **42**, 608 (2007).
[26] C. Wittneven, R. Dombrowski, M. Morgenstern, and R. Wiesendanger, Phys. Rev. Lett. **81**, 5616 (1998).
[27] J. A. Stroscio, R. M. Feenstra, and A. P. Fein, Phys. Rev. Lett. **57**, 2579 (1986).
[28] V. W. Brar *et al.*, Appl. Phys. Lett. **91**, 122102 (2007).
[29] G. M. Rutter *et al.*, Science **317**, 219 (2007).
[30] P. Lauffer *et al.*, Phys. Rev. B **77**, 155426 (2008).
[31] See EPAPS Document No. E-PRLTAO-102-050908 for supplementary figures and information on the methods. For more information on EPAPS, see http://www.aip.org/pubservs/epaps.html.
[32] I. Horcas *et al.*, Rev. Sci. Instrum. **78**, 013705 (2007).